

## Lattice thermal conductivity of nanostructured thermoelectric materials based on PbTe

Yee Kan Koh, C. J. Vineis, S. D. Calawa, M. P. Walsh, and David G. Cahill

Citation: *Appl. Phys. Lett.* **94**, 153101 (2009); doi: 10.1063/1.3117228

View online: <http://dx.doi.org/10.1063/1.3117228>

View Table of Contents: <http://apl.aip.org/resource/1/APPLAB/v94/i15>

Published by the [American Institute of Physics](#).

---

### Related Articles

Crystal orientation dependent thermoelectric properties of highly oriented aluminum-doped zinc oxide thin films  
*Appl. Phys. Lett.* **102**, 053507 (2013)

Comprehensive study of the metal-insulator transition in pulsed laser deposited epitaxial VO<sub>2</sub> thin films  
*J. Appl. Phys.* **113**, 043707 (2013)

Effect of oxygen vacancy distribution on the thermoelectric properties of La-doped SrTiO<sub>3</sub> epitaxial thin films  
*J. Appl. Phys.* **112**, 114104 (2012)

Measurement of the high-temperature Seebeck coefficient of thin films by means of an epitaxially regrown thermometric reference material  
*Rev. Sci. Instrum.* **83**, 093905 (2012)

Phase purity and the thermoelectric properties of Ge<sub>2</sub>Sb<sub>2</sub>Te<sub>5</sub> films down to 25nm thickness  
*J. Appl. Phys.* **112**, 014902 (2012)

---

### Additional information on *Appl. Phys. Lett.*

Journal Homepage: <http://apl.aip.org/>

Journal Information: [http://apl.aip.org/about/about\\_the\\_journal](http://apl.aip.org/about/about_the_journal)

Top downloads: [http://apl.aip.org/features/most\\_downloaded](http://apl.aip.org/features/most_downloaded)

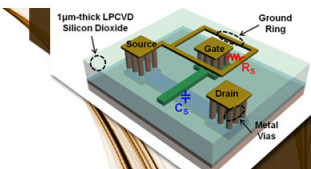
Information for Authors: <http://apl.aip.org/authors>

## ADVERTISEMENT

**AIP** | Applied Physics  
Letters


**EXPLORE WHAT'S  
NEW IN APL**

**SUBMIT YOUR PAPER NOW!**



**SURFACES AND  
INTERFACES**

Focusing on physical, chemical, biological, structural, optical, magnetic and electrical properties of surfaces and interfaces, and more...



**ENERGY CONVERSION  
AND STORAGE**

Focusing on all aspects of static and dynamic energy conversion, energy storage, photovoltaics, solar fuels, batteries, capacitors, thermoelectrics, and more...

# Lattice thermal conductivity of nanostructured thermoelectric materials based on PbTe

Yee Kan Koh,<sup>1,a)</sup> C. J. Vineis,<sup>2,3</sup> S. D. Calawa,<sup>2</sup> M. P. Walsh,<sup>2</sup> and David G. Cahill<sup>1</sup>

<sup>1</sup>Department of Materials Science and Engineering and Materials Research Laboratory, University of Illinois, Urbana, Illinois 61801, USA

<sup>2</sup>Lincoln Laboratory, Massachusetts Institute of Technology, Lexington, Massachusetts 02420, USA

<sup>3</sup>Wakonda Technologies, Woburn, Massachusetts 01801, USA

(Received 23 February 2009; accepted 19 March 2009; published online 14 April 2009)

We report the through-thickness lattice thermal conductivity  $\Lambda_l$  of  $(\text{PbTe})_{1-x}/(\text{PbSe})_x$  nanodot superlattices (NDSLs) over a wide range of periods  $5 \text{ nm} \leq h \leq 50 \text{ nm}$ , compositions  $0.15 \leq x \leq 0.25$ , growth temperatures  $550 \text{ K} \leq T_g \leq 620 \text{ K}$ , and growth rates  $1 \mu\text{m h}^{-1} \leq R \leq 4 \mu\text{m h}^{-1}$ . All of our measurements approach  $\Lambda_l$  of bulk homogenous  $\text{PbTe}_{1-x}\text{Se}_x$  alloys with the same average composition. For  $5 \text{ nm} \leq h \leq 50 \text{ nm}$ ,  $\Lambda_l$  is independent of  $h$ ; a result we attribute to short mean-free paths of phonons in PbTe and small acoustic impedance mismatch between PbTe/PbSe. We alloyed the PbTe layers of four NDSLs with SnTe up to a mole fraction  $y=18\%$ ;  $\Lambda_l$  is reduced by  $<25\%$ .  
© 2009 American Institute of Physics. [DOI: 10.1063/1.3117228]

Direct conversion of thermal and electrical energy by solid-state thermoelectric devices has attracted the attention of scientists and engineers since the advent of the semiconductor era in the 1950s. The dimensionless figure of merit for thermoelectric energy conversion<sup>1</sup> is  $ZT=S^2\sigma T/\Lambda$ , where  $S$  is the Seebeck coefficient,  $\sigma$  is the electrical conductivity,  $T$  is the absolute temperature, and  $\Lambda$  is the total thermal conductivity;  $ZT \approx 1$  for current commercial thermoelectric devices. Nanostructured semiconductors have been widely investigated as a route for increasing  $ZT$  through possible enhancement of the power factor  $S^2\sigma$  or the reduction of the thermal conductivity of the lattice  $\Lambda_l = \Lambda - \Lambda_e$ , where  $\Lambda_e$  is the thermal conductivity of the electronic system. In most cases, reductions of  $\Lambda_l$  by nanostructuring are thought to be more significant than enhancements of  $S^2\sigma$ .

Nanodot superlattices (NDSLs)<sup>1,2</sup> are an important class of nanostructured semiconductors. NDSLs are epitaxially grown thin films that contain nanoscale inclusions of a second phase, for example, PbSe embedded in PbTe. The nanoscale inclusions are produced by the Stranski–Krastinov growth mode of the PbSe layer. (The term “nanodot superlattices” is sometimes used interchangeably with the term “quantum dot superlattices” but we use “nanodots” to signify that band offsets are probably not sufficient to create carrier confinement near room temperature.) In 2002, Harman *et al.*<sup>1</sup> reported  $ZT=1.6$  at  $T=300 \text{ K}$  for PbTe/PbSe NDSLs;  $ZT$  was determined by measuring the maximum temperature change produced by a thermoelectric device where one leg of the devices was the NDSL and the other leg of the device was a gold wire. This factor of 3 enhancement in  $ZT$  compared to the best homogeneous PbTe-based alloys was attributed to the effects of the embedded nanodots that increased  $S^2\sigma$  and significantly decreased  $\Lambda_l$ . Recently however, studies<sup>3</sup> of the electrical properties of a large number of  $(\text{PbTe})_{1-x}/(\text{PbSe})_x$  NDSLs have shown that the power factor  $S^2\sigma$  of PbTe/PbSe NDSLs is actually reduced by  $\approx 30\%$  compared to bulk PbTe. In what follows, we show that the lattice thermal conductivity  $\Lambda_l$  of NDSLs also does not ben-

efit from nanostructuring by as much as was previously thought; in fact,  $\Lambda_l$  of NDSLs is similar to  $\Lambda_l$  of homogeneous  $\text{PbTe}_{1-x}\text{Se}_x$  alloys<sup>4</sup> with the same average composition. Using data for the in-plane power factor  $S^2\sigma$  and the through-thickness thermal conductivity  $\Lambda$ , we calculate a maximum  $ZT$  of 0.6 at 300 K, only 30% larger than well-optimized  $n$ -type PbTe ( $ZT \approx 0.45$ ).

We grew NDSLs by molecular beam epitaxy<sup>3</sup> on single-crystal (111)  $\text{BaF}_2$  or  $\text{CaF}_2$  substrates. For  $\text{CaF}_2$  substrates, a  $0.5 \mu\text{m}$  PbSe buffer layer was grown before the deposition of the NDSLs to improve the morphology. The total thickness of the NDSL films is  $1\text{--}10 \mu\text{m}$ . The growth temperature, measured by a pyrometer, was  $548\text{--}623 \text{ K}$  and the growth rate was  $1\text{--}4 \mu\text{m h}^{-1}$ . The NDSLs were intentionally doped using  $\text{Bi}_2\text{Te}_3$  ( $n$ -type) or  $\text{Na}_2\text{Te}$  ( $p$ -type).

We grew three kinds of superlattices: (1) NDSLs with a constant superlattice period in the range of  $5\text{--}50 \text{ nm}$ , (2) alternating-period NDSLs with two different periods ( $6.8$  and  $9 \text{ nm}$ ,  $12$  and  $16 \text{ nm}$ , and  $15$  and  $19 \text{ nm}$ ) alternating through the thickness of the film, and (3) a multiple-period NDSL with a sequence of six periods ( $11.5$ ,  $15.3$ ,  $19.2$ ,  $23$ ,  $19.2$ , and  $15.3 \text{ nm}$ ) that repeat through the film. In four additional samples, the PbTe layers were alloyed with SnTe to a maximum mole fraction of 18%. To calibrate our system, we measured the beam-equivalent-pressures of PbTe, PbSe and SnTe and the respective film thicknesses by cross-section Nomarski microscopy and Fourier transform infrared spectroscopy.

We measure the total thermal conductivity  $\Lambda$  in the through-thickness direction by time-domain thermoreflectance.<sup>5–7</sup> Prior to the measurements, the samples are coated with  $\approx 100 \text{ nm}$  thick Al films by magnetron sputter deposition. The  $1/e^2$  radii of the pump and probe beam at the sample surface are  $15 \mu\text{m}$ . The total laser power incident on the sample is  $<12 \text{ mW}$ , creating steady-state temperature rises of  $<10 \text{ K}$ . As carriers might be depleted near the surface of the samples, we use a modulation frequency of  $1 \text{ MHz}$  to reduce the sensitivity of our measurements to the thermal conductivity near the surface. The surface morphology of the NDSL samples shows significant roughness; thus, we employ a newly developed two-tint approach<sup>8</sup> to reject

<sup>a)</sup>Electronic mail: ykohl@mrl.uiuc.edu.

diffusely scattered light from the pump beam. We analyze the data following procedures described in Ref. 9, taking into account changing of the radius of the pump beam at different relative delay time between the pump and probe pulses.<sup>10</sup>

We determine the concentration and in-plane mobility of the charge carriers from Hall measurements using a van der Pauw geometry. The in-plane Seebeck coefficients are determined from simultaneous voltage and temperature measurements at two small pressed In contacts on the samples as the samples are sandwiched between a hot rod and a cold rod.<sup>3</sup> The mobility and Seebeck coefficients of the NDSLs are similar to values reported in Ref. 3 and are not reported here. The electronic contribution  $\Lambda_e$  to thermal conductivity is calculated from the measured electrical conductivity using the Wiedemann–Franz law and reduced Lorenz numbers<sup>3</sup> for nondegenerate electrons or holes in PbTe;  $\Lambda_l = \Lambda - \Lambda_e$ . To test the validity of this approach, we measured a highly *n*-doped ( $1.6 \times 10^{19} \text{ cm}^{-3}$ ) molecular beam epitaxy (MBE)-grown PbTe epitaxial film and found  $\Lambda = 3.5$ ,  $\Lambda_e = 1.1$ , and  $\Lambda_l = 2.4 \text{ W m}^{-1} \text{ K}^{-1}$ ; close to  $\Lambda_l = 2.0 \text{ W m}^{-1} \text{ K}^{-1}$  of bulk<sup>11</sup> PbTe and  $\Lambda_l = 2.5 \text{ W m}^{-1} \text{ K}^{-1}$  of epitaxial<sup>12</sup> PbTe.

We emphasize that our measurements of the total thermal conductivity  $\Lambda$  are in the through-thickness direction while the electrical conductivity  $\sigma$  is measured in the in-plane direction. PbTe and PbSe have cubic crystal structures; therefore,  $\Lambda$  and  $\sigma$  reduce to scalars for homogenous crystals. For a nanodot superlattice, some degree of anisotropy of  $\Lambda$  and  $\sigma$  might be created by the layering of the nanodots within the PbTe matrix. Transmission electron microscopy shows that the nanodots do not, in most cases, form well-defined layers. This fact, combined with the observed lack of  $\Lambda_l$  dependence on superlattice period, leads us to the conclusion that anisotropy in  $\Lambda$  and  $\sigma$  are insignificant compared to the uncertainties associated with calculating the Lorenz number.

We summarize the effects of period  $h$ , composition  $x$ , growth temperature  $T_g$ , and growth rate  $R$  on  $\Lambda_l$  of  $(\text{PbTe})_{1-x}/(\text{PbSe})_x$  NDSLs in Fig. 1;  $\Lambda_l$  varies with the mole fraction of PbSe  $x$  but we have not been able to identify any systematic variations with superlattice period or growth conditions. Data for PbTe-based planar superlattices<sup>12,13</sup> are included in Fig. 1(a) for comparison. To determine  $\Lambda_l$  of the samples studied in Refs. 12 and 13, we calculated  $\Lambda_e$  using the reduced Lorenz numbers of Ref. 3. (We disregarded one previous study that reported a strong dependence<sup>14</sup> of  $\Lambda_l$  of PbTe/PbTe<sub>0.75</sub>Se<sub>0.25</sub> planar superlattices on superlattice period; we concluded that the measurements reported in Ref. 14 were unreliable because the authors found unreasonably high values of  $\Lambda_l$  for PbTe and PbTe<sub>0.85</sub>Se<sub>0.15</sub> of 8.3 and 3.6  $\text{W m}^{-1} \text{ K}^{-1}$ , respectively.) We find that  $\Lambda_l$  of both PbTe/PbSe NDSLs and planar superlattices are similar to  $\Lambda_l$  of bulk homogeneous PbTe<sub>1-x</sub>Se<sub>x</sub> alloys<sup>4</sup> with the same average composition.

We note that our  $\Lambda_l$  values in Fig. 1 are significantly higher than the estimation by Harman *et al.*<sup>1</sup> and a lower-bound measurement<sup>15</sup> of total thermal conductivity ( $\Lambda = 0.85 \pm 0.13 \text{ W/m K}$  at  $\sim 360 \text{ K}$ ) taken on a 95  $\mu\text{m}$  thick NDSL film metallized on both sides, using an apparatus based on one-dimensional heat flow in vacuum.<sup>16</sup> Reasons for the discrepancy are unclear to the authors.

We attribute the lack of dependence of  $\Lambda_l$  on superlattice period to the short mean-free-paths for heat carrying

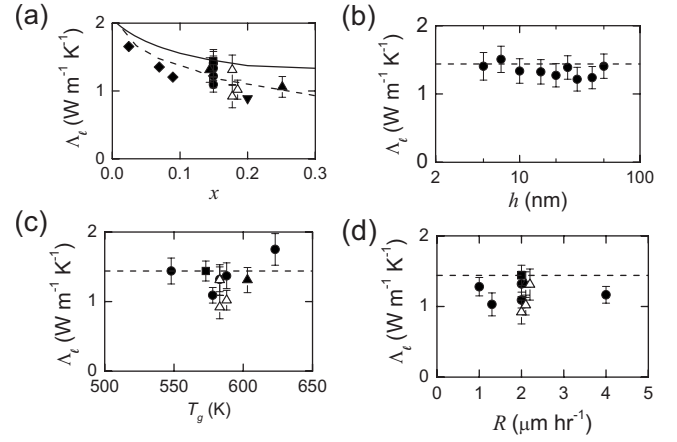


FIG. 1. Through-thickness lattice thermal conductivity  $\Lambda_l$  of single-period (circles), alternating-period (up triangles), and multiple-period (squares)  $(\text{PbTe})_{1-x}/(\text{PbSe})_x$  NDSLs plotted as a function of (a) mole fraction  $x$  of PbSe; (b) superlattice period  $h$ ; (c) growth temperature  $T_g$ ; and (d) growth rate  $R$ . Solid symbols are for *n*-doped samples and open symbols are for *p*-doped samples. Data points with error bars are from this study; data points without error bars are drawn from the literature. If not otherwise specified,  $x \approx 0.16$ ,  $h \approx 15 \text{ nm}$ ,  $573 \text{ K} < T_g < 603 \text{ K}$ , and  $R \approx 2 \mu\text{m h}^{-1}$ . In part (a),  $5 \text{ nm} < h < 30 \text{ nm}$ ; and the in-plane  $\Lambda_l$  of PbTe/PbTe<sub>0.8</sub>Se<sub>0.2</sub> superlattices (diamonds) (Ref. 12) and cross-plane  $\Lambda_l$  of a PbTe<sub>0.7</sub>Se<sub>0.3</sub>/PbTe<sub>0.9</sub>Se<sub>0.1</sub> superlattice (down triangle) (Ref. 13) are included for comparison. The dashed and solid lines in (a) are the measured (Ref. 4) and calculated [using  $\Gamma$  from Eq. (1)]  $\Lambda_l$  of bulk PbTe<sub>1-x</sub>Se<sub>x</sub> alloys, respectively. The dashed lines in (b), (c), and (d) are  $\Lambda_l$  of an MBE-grown PbTe<sub>0.85</sub>Se<sub>0.15</sub> thin film and are included as a baseline for comparisons.

phonons in PbTe and the relatively small difference in acoustic impedance between PbTe and PbSe; for example, for longitudinal acoustic modes in the (100) direction, the impedance mismatch is only 1.1. (Measured in the same way, the acoustic mismatch of AlAs/GaAs and Si/Ge are 1.2 and 1.3, respectively.) Using the Debye–Callaway model described below, we find that half of the heat is carried by phonons with mean-free-path  $< 19 \text{ nm}$  in PbTe, compared to  $< 300$  and  $< 140 \text{ nm}$  in Si and GaAs. In other words, heat carrying phonons in PbTe are already strongly scattered by anharmonic phonon-phonon interactions and additional scattering of phonons by nanodots is relatively small.

We attempted to decrease the lattice thermal conductivity further by alloying the PbTe layers of NDSLs with SnTe. At a composition of 18% SnTe, the reduction in  $\Lambda_l$  is 25%; a similar reduction is found in the homogenous Pb<sub>1-m</sub>Sn<sub>m</sub>Te<sub>1-n</sub>Se<sub>n</sub> alloys<sup>17,18</sup> with similar compositions, see Fig. 2.

To provide a baseline for comparisons and to help guide future work, we calculate the thermal conductivity of a homogeneous PbTe-based alloy using a model that includes phonon scattering by point defects. The cross section for phonon scattering by point defects is characterized by the parameter  $\Gamma$  that has contributions<sup>19</sup> from variations in the atomic masses ( $\Gamma_{\text{mass}}$ ), and variations in the length and strength of the bonds ( $\Gamma_{\text{bond}}$ );  $\Gamma = \Gamma_{\text{mass}} + \Gamma_{\text{bond}}$ . We follow Ref. 19 and derive an expression of  $\Gamma$  for an  $A_{1-m}B_mC_{1-n}D_n$  quaternary alloy with  $m \ll 1$  and  $n \ll 1$ ,

$$\Gamma_{\text{mass}} = \frac{m(1-m)}{2} \left( \frac{M_A - M_B}{M_{AB}} \right)^2 + \frac{n(1-n)}{2} \left( \frac{M_C - M_D}{M_{CD}} \right)^2, \quad (1a)$$



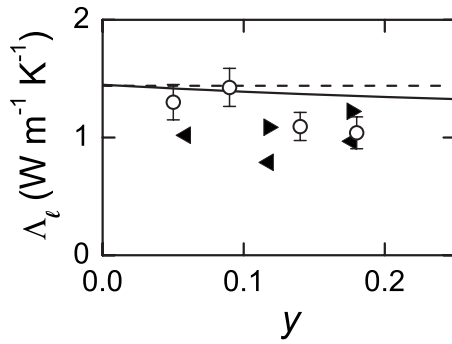


FIG. 2. Through thickness lattice thermal conductivity  $\Lambda_l$  of  $p$ -doped  $(\text{Pb}_{1-y}\text{Sn}_y\text{Te})_{0.85}/(\text{PbSe})_{0.15}$  NDSLs (open circles), compared to  $\Lambda_l$  of bulk  $\text{Pb}_{1-m}\text{Sn}_m\text{Te}_{0.85}\text{Se}_{0.15}$  alloys ( $m=0.85y$ ) from Ref. 17 (left triangles) and Ref. 18 (right triangles). The superlattice periods are  $h=18$  nm. The dashed line is  $\Lambda_l$  of an MBE-grown  $\text{PbTe}_{0.85}\text{Se}_{0.15}$  thin film and is included as a baseline for comparisons. The solid line is the lattice thermal conductivity of the  $\text{Pb}_{1-z}\text{Sn}_z\text{Te}_{0.85}\text{Se}_{0.15}$  alloys calculated using the Debye-Callaway model, using  $\Gamma$  from Eq. (1).

$$\Gamma_{\text{bond}} = 2\epsilon m(1-m) \left( \frac{\delta_{AC} - \delta_{BC}}{\delta_{ABC}} \right)^2 + 2\epsilon n(1-n) \times \left( \frac{\delta_{AC} - \delta_{AD}}{\delta_{ACD}} \right)^2, \quad (1b)$$

where  $M_i$  is the mass of atom  $i$ ,  $M_{AB}=mM_B+(1-m)M_A$ ,  $M_{CD}=nM_D+(1-n)M_C$ ,  $\delta_{ij}$  is the lattice constant of unperturbed lattice  $ij$ ,  $\delta_{ABC}=m\delta_{BC}+(1-m)\delta_{AC}$ ,  $\delta_{ACD}=n\delta_{AD}+(1-n)\delta_{AC}$ , and  $\epsilon$  is a constant depending on the elastic properties of the matrix;  $\epsilon=65$  for PbTe.<sup>17</sup> We derive  $\Gamma_{\text{mass}}=0.010$  and  $\Gamma_{\text{bond}}=0.046$  for  $\text{PbTe}_{0.85}\text{Se}_{0.15}$ ;  $\Gamma_{\text{mass}}=0.024$  and  $\Gamma_{\text{bond}}=0.053$  for  $\text{Pb}_{0.85}\text{Sn}_{0.15}\text{Te}_{0.85}\text{Se}_{0.15}$ . This calculation suggests that phonon scattering by point defects in most PbTe alloys is controlled by variations in bond strengths and lengths rather than variations in the atomic masses. We construct a Debye-Callaway model similar to what we developed previously for III-V materials.<sup>10,20</sup> We fix the relative anharmonic scattering strengths of umklapp and normal processes, and obtain the absolute strengths from a fit to  $\Lambda_l$  of bulk PbTe.<sup>11</sup> We use Eq. (1) to calculate  $\Gamma$ . We include only Debye phonons with frequencies below the frequency of phonons at Brillouin zone boundaries;  $\sim 10\%$  of the available phonon modes are accounted for by this approach. We estimate the thermal conductivity of the unaccounted phonons from the minimum thermal conductivity,<sup>21</sup>  $\Lambda_{\text{min}} \approx 0.36 \text{ W m}^{-1} \text{ K}^{-1}$ . We add  $\Lambda_{\text{min}}$  to the calculations of the Debye-Callaway model. The results are plotted as solid lines in Figs. 1(a), 2, and 3. The agreement between the calculations and the measurements are satisfactory for a broad range of  $\Gamma$ , see Fig. 3.

In conclusion, PbSe nanodots do not reduce  $\Lambda_l$  of PbTe-based NDSLs below the alloy limit. The  $\Lambda_l$  of PbTe-based NDSLs is similar to  $\Lambda_l$  of homogenous alloys with the same average composition and can be readily estimated using a simple model taking into account scattering of phonons by point defects. Our work provides guidelines for future work on nanostructured thermoelectrics based on PbTe.

The work at the University of Illinois (UIUC) was supported by ONR (Grant No. N00014-07-1-0190). Sample characterization used the facilities of the Center of Microanalysis of Materials which is partially supported by the

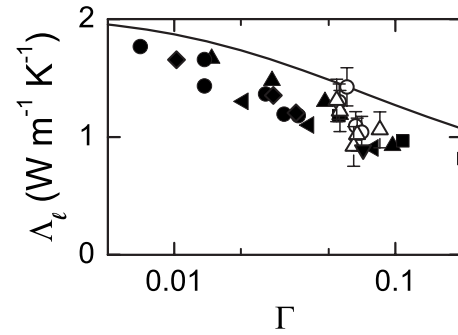


FIG. 3. Compilation of the lattice thermal conductivity  $\Lambda_l$  of  $(\text{PbTe})_{1-x}/(\text{PbSe})_x$  NDSLs (open up triangles) and  $(\text{Pb}_{1-y}\text{Sn}_y\text{Te})_{0.85}/(\text{PbSe})_{0.15}$  NDSLs (open circles) measured in this work with comparison to  $\text{PbTe}/\text{PbTe}_{0.8}\text{Se}_{0.2}$  superlattices (diamonds, Ref. 12) and  $\text{PbTe}_{0.9}\text{Se}_{0.1}$  superlattices (down triangle, Ref. 13); bulk  $\text{PbTe}_{1-x}\text{Se}_x$  (solid up triangles, Ref. 4),  $\text{Pb}_{1-m}\text{Sn}_m\text{Te}$  (solid circles, Refs. 17 and 22),  $\text{Pb}_{1-m}\text{Ge}_m\text{Te}$  (left triangles, Refs. 17 and 23) and  $\text{PbTe}_{1-n}\text{S}_n$  (squares, Ref. 17) alloys.  $\Gamma$  is the impurity scattering cross section discussed in text, see Eq. (1). The solid line is the calculations of the Debye-Callaway model for a hypothetical PbTe solid with the corresponding impurity scattering cross section  $\Gamma$ .

U.S. Department of Energy under Grant No. DEFG02-91ER45439. The MIT Lincoln Laboratory portion of this work was sponsored by ONR under Air Force Contract No. FA8721-05-0002.

- <sup>1</sup>T. C. Harman, P. J. Taylor, M. P. Walsh, and B. E. LaForge, *Science* **297**, 2229 (2002).
- <sup>2</sup>T. C. Harman, P. J. Taylor, D. L. Spears, and M. P. Walsh, *J. Electron. Mater.* **29**, L1 (2000).
- <sup>3</sup>C. J. Vineis, T. C. Harman, S. D. Calawa, M. P. Walsh, R. E. Reeder, R. Singh, and A. Shakouri, *Phys. Rev. B* **77**, 235202 (2008).
- <sup>4</sup>A. V. Ioffe and A. F. Ioffe, *Izv. Akad. Nauk SSSR, Ser. Fiz.* **20**, 65 (1956).
- <sup>5</sup>C. A. Paddock and G. L. Eesley, *J. Appl. Phys.* **60**, 285 (1986).
- <sup>6</sup>D. A. Young, C. Thomsen, H. T. Grahn, H. J. Maris, and J. Tauc, in *Phonon Scattering in Condensed Matter*, edited by A. C. Anderson and J. P. Wolfe (Springer, Berlin, 1986), p. 49.
- <sup>7</sup>D. G. Cahill, W. K. Ford, K. E. Goodson, G. D. Mahan, A. Majumdar, H. J. Maris, R. Merlin, and S. R. Phillpot, *J. Appl. Phys.* **93**, 793 (2003).
- <sup>8</sup>K. Kang, Y. K. Koh, C. Chiritescu, X. Zheng, and D. G. Cahill, *Rev. Sci. Instrum.* **79**, 114901 (2008).
- <sup>9</sup>D. G. Cahill, *Rev. Sci. Instrum.* **75**, 5119 (2004).
- <sup>10</sup>Y. K. Koh and D. G. Cahill, *Phys. Rev. B* **76**, 075207 (2007).
- <sup>11</sup>E. D. Devyatkov and I. A. Smirnov, *Sov. Phys. Solid State* **3**, 1666 (1962).
- <sup>12</sup>H. Beyer, J. Nurnus, H. Böttner, A. Lambrecht, T. Roch, and G. Bauer, *Appl. Phys. Lett.* **80**, 1216 (2002).
- <sup>13</sup>D. G. Cahill, A. Bullen, and S.-M. Lee, *High Temp. - High Press.* **32**, 135 (2000).
- <sup>14</sup>J. C. Caylor, K. Cooley, J. Stuart, T. Colpitts, and R. Venkatasubramanian, *Appl. Phys. Lett.* **87**, 023105 (2005).
- <sup>15</sup>P. Mayer, "High-density thermoelectric power generation and nanoscale thermal metrology," Ph.D. thesis, Massachusetts Institute of Technology, 2007.
- <sup>16</sup>P. Mayer and R. J. Ram, 24th International Conference on Thermoelectrics, 19–23 June 2005 (unpublished), pp. 280–283.
- <sup>17</sup>G. T. Alekseeva, B. A. Efimova, L. M. Ostrovskaya, O. S. Serebryannikova, and M. I. Tsypin, *Sov. Phys. Semicond.* **4**, 1122 (1971).
- <sup>18</sup>E. A. Gurieva, P. P. Konstantinov, L. V. Prokof'eva, D. A. Pshenai-Severin, M. I. Fedorov, and Yu. I. Ravich, *Semiconductors* **40**, 763 (2006).
- <sup>19</sup>B. Abeles, *Phys. Rev.* **131**, 1906 (1963).
- <sup>20</sup>Y. K. Koh, Y. Cao, D. G. Cahill, and D. Jena, *Adv. Funct. Mater.* **19**, 610 (2009).
- <sup>21</sup>D. G. Cahill and R. O. Pohl, *Annu. Rev. Phys. Chem.* **39**, 93 (1988).
- <sup>22</sup>M. Orihashi, Y. Noda, L. Chen, and T. Hirai, *Mater. Trans. JIM* **41**, 1196 (2000).
- <sup>23</sup>I. Kudman, *Mettall. Trans.* **2**, 163 (1971).